Theoretical spectroscopic characterization at low temperatures of detectable sulfur-organic compounds: Ethyl mercaptan and dimethyl sulfide

M. L. Senent, C. Puzzarini, R. Domínguez-Gómez, M. Carvajal, and M. Hochlaf

Citation: The Journal of Chemical Physics **140**, 124302 (2014); doi: 10.1063/1.4868640

View online: http://dx.doi.org/10.1063/1.4868640

View Table of Contents: http://scitation.aip.org/content/aip/journal/jcp/140/12?ver=pdfcov

Published by the AIP Publishing

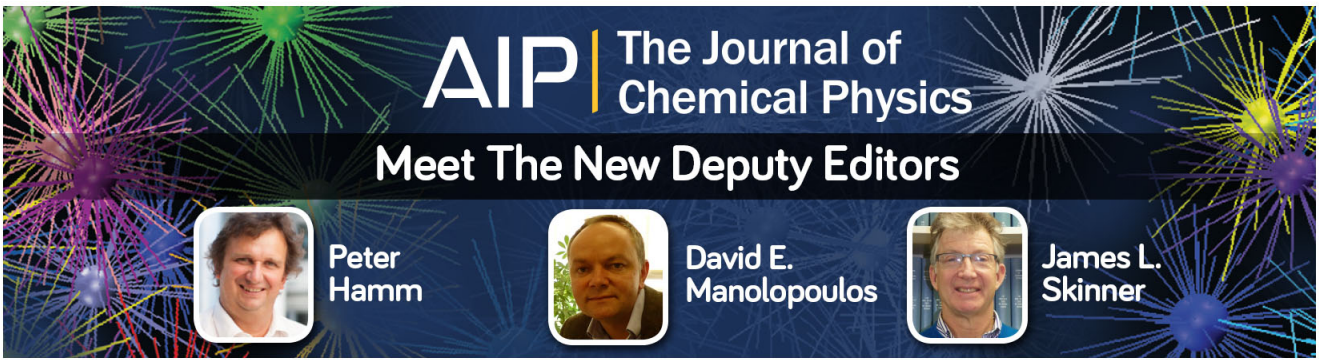

Theoretical spectroscopic characterization at low temperatures of detectable sulfur-organic compounds: Ethyl mercaptan and dimethyl sulfide

M. L. Senent,[1,a)] C. Puzzarini,[2,b)] R. Domínguez-Gómez,[3,c)] M. Carvajal,[4,d)] and M. Hochlaf[5,e)]

[1]*Departamento de Química y Física Teóricas, Instituto de Estructura de la Materia, IEM-C.S.I.C., Serrano 121, Madrid 28006, Spain*
[2]*Dipartimento di Chimica G. Ciamician, Università di Bologna, Via F. Selmi 2, I-40126 Bologna, Italy*
[3]*Doctora Vinculada IEM-CSIC, Departamento de Ingeniería Civil, Cátedra de Química, E.U.I.T. Obras Públicas, Universidad Politécnica de Madrid, Spain*
[4]*Departamento de Física Aplicada, Facultad de Ciencias Experimentales, Unidad Asociada IEM-CSIC-U.Huelva, Universidad de Huelva, 21071 Huelva, Spain*
[5]*Laboratoire de Modélisation et Simulation Multi Echelle, Université Paris-Est, MSME UMR 8208 CNRS, 5 Boulevard Descartes, 77454 Marne-la-Vallée, France*

(Received 14 January 2014; accepted 5 March 2014; published online 24 March 2014)

Highly correlated *ab initio* methods are used for the spectroscopic characterization of ethyl mercaptan ($CH_3CH_2{}^{32}SH$, ETSH) and dimethyl sulfide ($CH_3{}^{32}SCH_3$, DMS), considering them on the vibrational ground and excited torsional states. Since both molecules show non-rigid properties, torsional energy barriers and splittings are provided. Equilibrium geometries and the corresponding rotational constants are calculated by means of a composite scheme based on CCSD(T) calculations that accounts for the extrapolation to the complete basis set limit and core-correlation effects. The ground and excited states rotational constants are then determined using vibrational corrections obtained from CCSD/cc-pVTZ force-field calculations, which are also employed to determine anharmonic frequencies for all vibrational modes. CCSD(T) and CCSD force fields are employed to predict quartic and sextic centrifugal-distortion constants, respectively. Equilibrium rotational constants are also calculated using CCSD(T)-F12. The full-dimensional anharmonic analysis does not predict displacements of the lowest torsional excited states due to Fermi resonances with the remaining vibrational modes. Thus, very accurate torsional transitions are calculated by solving variationally two-dimensional Hamiltonians depending on the CH_3 and SH torsional coordinates of ethyl mercaptan or on the two methyl groups torsions of dimethyl-sulfide. For this purpose, vibrationally corrected potential energy surfaces are computed at the CCSD(T)/aug-cc-pVTZ level of theory. For ethyl mercaptan, calculations show large differences between the *gauche* (*g*) and *trans* (*t*) conformer spectral features. Interactions between rotating groups are responsible for the displacements of the *g*-bands with respect to the *t*-bands that cannot therefore be described with one-dimensional models. For DMS, the CCSD(T) potential energy surface has been semi-empirically adjusted to reproduce experimental data. New assignments are suggested for the methyl torsion bands of ETSH and a reassignment is proposed for the infrared bands of DMS (0 3 → 0 4 and 1 0 → 1 1). Our accurate spectroscopic data should be useful for the analysis of the microwave and far infrared spectra of ETSH and DMS recorded, at low temperatures, either in laboratory or in the interstellar medium.
 [http://dx.doi.org/10.1063/1.4868640]

INTRODUCTION

New astronomical observatories are performing detailed spectral line measurements of extraterrestrial sources. Given their capabilities, surveys covering large frequency ranges can contain many unidentified lines corresponding to new molecules or to vibrationally excited states of previously detected species. The resolution of the corresponding spectral confusion implies full assignment of astronomical spectra, which in turn requires a complete an accurate spectroscopic characterization at different temperatures of all the involved species.

Unfortunately, many species considered as detectable candidates are not well characterized. Molecular catalogs do not contain enough information concerning new molecules and vibrational excitations.[1] In particular, it turns out to be necessary to give special attention to non-rigid species for which large amplitude motions may interconvert different minima on the potential energy surfaces (PESs). Since these molecules display very low energy levels that can be

a)Author to whom correspondence should be addressed. Electronic mail: senent@iem.cfmac.csic.es
b)E-mail: cristina.puzzarini@unibo.it
c)E-mail: rosa.dominguez@upm.es
d)E-mail: miguel.carvajal@dfa.uhu.es
e)E-mail: Majdi.Hochlaf@u-pem.fr

populated at very low temperatures, they may exist in excited vibrational states in relatively hot sources, such as the hot molecular cores. It is worthwhile noting that many prebiotic molecules have been detected in these "hot cores."[2] "Hot core" models actually predict the existence of new prebiotic species.

Both molecules, ethyl mercaptan (ETSH) and dimethyl sulfide (DMS), are classified as detectable in the interstellar medium since they are sulfur analogs (S-analogs) of two important and abundant early discovered astrophysical molecules: ethanol (CH_3CH_2OH, ETOH) and dimethyl ether (CH_3OCH_3, DME). Usually, with a few exceptions,[3] the detection of S-bearing species follows the detection of the corresponding O-analog: the search for S-analogs of already detected species is a consistent strategy of astrophysicists.

The first detection of a sulfur-containing species, carbon sulfide (CS), occurred in 1971.[4] Although S is not one of the abundant cosmological elements (such as C, O, N, and H), it can play an important role in the chemical evolution of many sources. S-bearing abundance ratios have been previously proposed and used as chemical clocks.[5–7] To date, more than 20 different molecules containing S have been found, which is an unexpected large number given the small S/O abundance ratio (1/42). Methyl mercaptan, the S-analog of methanol, is the only sulfur-containing non-rigid molecule detected so far.[8] This validates the crucial importance of searching for ethyl mercaptan. Consequently, this non-rigid S-bearing molecule has become a target species for astrophysicists.

Both molecules, ETSH and DMS, show a non-rigid behavior. DMS has two equivalent methyl groups leading to nine equivalent minima, while ETSH has a unique methyl group, which is responsible for interconversion between three equivalent minima. In addition, for the latter, a second torsional coordinate, the thiol torsion (SH torsion), intertransforms two conformers, the *gauche* and *trans* forms. The couple of the torsional motions of ETSH generates a potential energy surface with nine minima. ETSH and DMS share many spectroscopic properties with their O-analogs ethanol and dimethylether. Both of them were already deeply investigated by some of the authors[9,10] and a detailed comparison is deserved.

Due to its relevance for atmospheric studies, DMS has been characterized since 1940.[11] This results into a large amount of theoretical and experimental data.[12] However, ETSH has been less investigated and a few, generally old information is available.[13–15] In 1948, the structure of the two conformers of ethyl mercaptan and the torsional barriers were investigated by Sheppard.[13] In 1968, Smith *et al.*[14] recorded the infrared spectrum of the *gauche* conformer in gas and condensed phases. The infrared vibrational spectrum was also explored by Manocha *et al.*,[16] Wolff and Szydlowski,[17] and very recently by Miller *et al.*,[15] who recorded the IR ETSH spectrum in the vicinity of the SH-stretching spectra with the band (at 2591 cm^{-1}). The Raman spectrum was studied by Durig *et al.*[18] and Richter and Schiel.[19] Inagaki *et al.*,[20] Manocha *et al.*,[16] and Durig *et al.*[18] observed torsional bands around 250 cm^{-1}. Rotational constants, torsional barriers (V_3 = 1329 cm^{-1}), and dipole moments were derived by Schmidt and Quade[21] using microwave spectroscopy. Theoretical papers on ETSH have also been published[22,23] using relatively low levels of theory and small basis sets.

The microwave spectrum of DMS was measured by Pierce and Hayashi,[24] Demaison *et al.*,[25] and Vacherand *et al.*[26] Recently, Niide and Hayashi[12] recorded lines for the ground and the excited torsional states, providing rotational parameters for various states and isotopologues. Further studies on the Raman and IR vibrational spectra were carried out by Fonteyne,[11] Durig and Griffin,[27] and Durig *et al.*[28] The latter authors focused their investigations on torsional features, and estimated the methyl torsional barrier to be 746 cm^{-1}. Several theoretical papers were published.[29,30] In particular, Senent *et al.*[30] employed Møller-Plesset theory to explore the potential energy surface and then the spectrum in the far infrared region.

In this paper, we use highly correlated *ab initio* methods to perform the spectroscopic characterization of the most abundant isotopologues of ethyl mercaptan ($CH_3CH_2{}^{32}SH$, ETSH) and dimethyl sulfide ($CH_3{}^{3}SCH_3$, DMS), considering them on the vibrational ground and excited torsional states. The main aim is to help the interpretation of future experimental spectroscopic studies by providing very accurate rotational and torsional parameters, which can be used to support spectral assignments as starting point in the fitting procedure. In detail, the present paper, we perform a complete theoretical spectroscopic characterization of ETSH and DMS following two different procedures:

(1) Structural and rotational parameters at equilibrium and on the vibrational ground and excited states are determined by means of a composite approach,[31,32] and using the newly implemented explicitly correlated coupled-cluster technique.
(2) All torsional parameters (barriers, energy levels, and splittings) are calculated following the variational procedure of Senent and co-workers, implemented in the code ENEDIM.[33]

Both procedures imply the use of highly correlate *ab initio* methods in conjunction with very large basis sets, even accounting for extrapolation to the complete basis-set (CBS) limit. Details of the theoretical and computational procedures are described in the sections titled Equilibrium structures and rotational parameters and Torsional analysis. For DMS, for which enough experimental data are available, a final semi-empirical adjustment of the effective torsional Hamiltonian parameters is carried out. For both species, we perform a thorough comparison of the spectroscopic parameters with those of the corresponding O-analogs.[9,10] The effect of the O → S substitution is thus detailed, as it was done in previous papers where couples of analogs were treated and compared.[34–36]

THEORETICAL AND COMPUTATIONAL DETAILS

As mentioned above, the present spectroscopic characterization follows two different procedures: the first one is devoted to the determination of molecular structures and rotational constants, while the second one represents a torsional analysis.

Equilibrium structures and rotational parameters

For the equilibrium structure determination, we use a rigorous approach based on additivity at an energy-gradient level,[31,32] as implemented in the CFOUR package.[37] The contributions taken into account are: the Hartree-Fock self-consistent-field (HF-SCF) energy extrapolated to the basis-set limit, the valence correlation energy at the coupled-cluster level of theory employing the singles and doubles approximation (CCSD) augmented by a perturbative treatment of triple excitations, CCSD(T),[38] extrapolated to the basis-set limit as well, and the core-valence-correlation correction. The correlation-consistent cc-pV*n*Z (n = T-Q) and cc-pCVTZ basis sets[39–41] were employed. In the following, these sets will be shortly denoted as V*n*Z and CVTZ, respectively.

The energy gradient used in the geometry optimization is therefore given by

$$\frac{dE_{CBS+CV}}{dx} = \frac{dE^{\infty}(HF-SCF)}{dx} + \frac{d\Delta E^{\infty}(CCSD(T))}{dx} + \frac{d\Delta E(CV)}{dx}, \quad (1)$$

where dE^{∞}(HF-SCF)/dx and $d\Delta E^{\infty}$(CCSD(T))/dx are the energy gradients obtained using for the HF-SCF energy the exponential extrapolation formula of Feller[42] and the n^{-3} extrapolation scheme for the CCSD(T) correlation contribution,[43] respectively. In the equation above, n = T, Q, and 5 were chosen for the HF-SCF extrapolation, whereas n = T and Q were used for CCSD(T). Core-valence-correlation effects are included by adding the corresponding correction dΔE(CV)/dx, with the energy correction, E(CV), being obtained as the difference between the all-electron and frozen-core CCSD(T) energies using the core-valence CVTZ basis set.[40,41] The overall best-estimated geometries, accounting for extrapolation to the CBS limit and core-correlation corrections, are denoted as CCSD(T)/CBS(T,Q) +CV(CT).

Spectroscopic parameters, like vibrational corrections to rotational constants and centrifugal-distortion constants, were obtained by means of second-order vibrational perturbation theory (VPT2).[44] This requires a cubic force field to be evaluated. The latter was computed at the CCSD/VTZ level. The harmonic part was obtained using analytic second derivatives,[45] whereas the cubic force field was determined in a normal-coordinate representation via numerical differentiation of the harmonic force constants.[46,47]

The equilibrium rotational constants were straightforwardly derived from the best-estimated structure described above. In a second step, to obtain the ground- and excited-state rotational constants, the equilibrium rotational constants were corrected for vibrational effects according to the following expression:[44,48–50]

$$B_v^i = B_e^i - \sum_r \alpha_r^i \left(v_r + \frac{d_r}{2}\right), \quad (2)$$

where the α_r^i are the vibration-rotation interaction constants, with the sum running over all normal modes and v_r and d_r being the corresponding vibrational quantum number and mode degeneracy; i denotes the inertial axis.

In addition to the vibration-rotation interaction constants, the computed force fields enabled the determination of the quartic and sextic centrifugal-distortion constants by means of VPT2.[44,48] For the former parameters, the required harmonic force field was also evaluated at the CCSD(T)/VTZ level. The recent implementation of sextic centrifugal-distortion constants in the CFOUR quantum-chemical program package is described in Ref. 52.

For comparison purposes, equilibrium structures and equilibrium rotational constants were computed using the explicitly correlated coupled-cluster method CCSD(T)-F12[52,53] as implemented in MOLPRO.[54] Here, the H, S, and C atoms were described using the cc-pVTZ-F12 (denoted in the following as VTZ-F12) explicitly correlated basis set,[55] together with the corresponding auxiliary basis sets and density fitting functions[56–58] and the default CABS(OptRI) basis sets of Yousaf and Peterson.[59] As it is well established in the literature, the CCSD(T)-F12/VTZ-F12 level of theory reaches the standard CCSD(T)/AV5Z accuracy,[39–60] with a strong reduction of computational efforts by about two orders of magnitude in CPU time and disk.[61–66] Note that the explicitly correlated coupled-cluster methodology presently used in conjunction with the VTZ-F12 basis set allows to describe the correlation effects due to valence electrons.

Torsional analysis

Far infrared and Raman frequencies of ETSH and DMS were determined variationally assuming very small, almost negligible, interactions between the torsional large amplitude torsional modes and the remaining vibrations.

For this purpose, the torsional energy levels were obtained by solving the following two-dimensional Hamiltonian,[67,68]

$$\hat{H}(q_i,q_j) = -\sum_{i=1}^{2}\sum_{j=1}^{2}\left(\frac{\partial}{\partial q_i}\right) B_{q_iq_j}(q_i,q_j)\left(\frac{\partial}{\partial q_j}\right) + V(q_i,q_j) + V'(q_i,q_j) + V^{ZPVE}(q_i,q_j), \quad (3)$$

which depends on two independent coordinates q_i and q_j. For ETSH, q_i and q_j are identified as the CH_3 torsion (θ) and the SH torsion (α), respectively (Figure 1(a)). In DMS, both coordinates correspond to methyl internal rotations (θ_1 and θ_2) (Figure 1(b)).

In Eq. (3), V(q_i, q_j) represents the two-dimensional potential energy surface (2D-PES). In this paper, the required PESs are determined from the CCSD(T)/AVTZ[39,60] total electronic energies for a number NS of selected geometries defined for different values of the independent coordinates. NS depends on the molecular symmetry: NS = 26 for ETSH and NS = 7 for DMS. For each NS structure, 3Na-6-n internal coordinates (Na = number of atoms, n = 2 dihedral angles) were optimized at the CCSD/AVTZ level, which is a way to partially consider the small interactions with remaining vibrational modes. These electronic

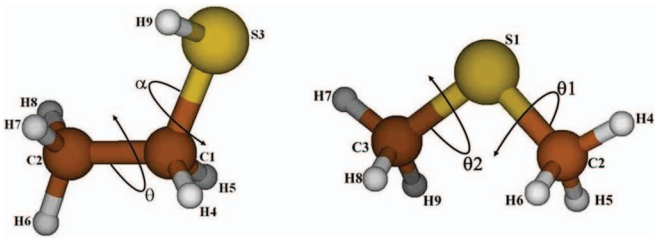

FIG. 1. Minimum energy structures and torsional coordinates, q_i and q_j: (left) *gauche*-methyl mercaptan ($q_1 = \theta$, $q_j = \alpha$); (right) dimethyl sulfide ($q_1 = \theta_1$, $q_j = \theta_2$).

structure calculations have been performed with the Gaussian 09 package.[69]

In Eq. (3), B_{qiqj} and $V'(q_i, q_j)$ represent the kinetic energy parameters and the Podolsky pseudopotential, respectively. For their definitions, the readers are referred to Ref. 67. For each NS structure, these parameters were determined with the code ENEDIM.[33] Subsequently, they were fitted to symmetry adapted series formally identical to the 2D-PESs.

The torsional Hamiltonian of Eq. (3) contains a vibrational correction, $V^{ZPVE}(q_i, q_2)$, that can be defined as the torsional dependence of the contribution of the 3Na-6-n neglected modes on the zero point vibrational energy (ZPVE). Usually, this correction improves the results, as demonstrated by Császár *et al.*[70] For a given geometry, the ZPVE correction can be calculated by means of the following equation:

$$E^{ZPVE}(q_i, q_j) = \sum_{k=3}^{3N-6} \frac{\omega_k}{2}, \tag{4}$$

where ω_k are the harmonic frequencies of the neglected modes. Then, V^{ZPVE} is obtained from a linear fit of E^{ZPVE} to symmetry adapted series. For the purpose of the present paper, E^{ZPVE} was calculated at the MP2/AVTZ level, which can be considered enough accurate and computationally efficient.

The energy levels were determined variationally using as trial function symmetry-adapted eigenvectors of double Fourier series, according to the procedures implemented in ENEDIM.[33] Three criteria were employed for the labeling of the level:

(i) Levels are labeled using the symmetry representations of the G_6 and G_{36} molecular symmetry groups (MSG) of ETSH and DMS (as for ethanol[9] and dimethyl-ether,[10] respectively).

(ii) Levels are assigned to the different conformers on the basis of the probability integrals involving the torsional wavefunctions $\psi(\theta,\alpha)$,

$$P = \int_{0,-\alpha}^{360,\alpha} \psi_i^*(\theta, \alpha)\psi_i(\theta, \alpha)d\theta d\alpha. \tag{5}$$

(iii) Vibrational quanta are assigned to the levels using the expectation values,

$$\begin{aligned} P_\theta &= \langle \psi_i(\theta, \alpha)|\hat{H}(\theta)|\psi_i(\theta, \alpha)\rangle, \\ P_\alpha &= \langle \psi_i(\theta, \alpha)|\hat{H}(\alpha)|\psi_i(\theta, \alpha)\rangle \end{aligned} \tag{6}$$

of the one-dimensional operators $\hat{H}(\theta)$ and $\hat{H}(\alpha)$

$$\hat{H}(\theta) = -\left(\frac{\partial}{\partial\theta}\right) B_\theta \left(\frac{\partial}{\partial\theta}\right) + V(\theta),$$

$$\hat{H}(\alpha) = -\left(\frac{\partial}{\partial\alpha}\right) B_\alpha \left(\frac{\partial}{\partial\alpha}\right) + V(\alpha).$$

The steps summarized above are relevant in the procedure for ETSH, for which a large density of states close to the minima is obtained.

RESULTS AND DISCUSSION

Molecular structure and rotational constants

ETSH consists of two conformers, the *gauche* (*g*-ETSH) and *trans* (*t*-ETSH) forms of C_1 and C_s symmetries, respectively, whereas DMS presents a single C_{2V} conformer. The corresponding equilibrium structures were obtained by geometry optimizations at different levels of theory: CCSD/AVTZ, CCSD(T)/AVTZ, CCSD(T)-F12/VTZ-F12, and CCSD(T)/CBS(T,Q)+CV(CT). The CCSD(T)/CBS(T,Q)+CV(CT) structural parameters, which are expected to be the most accurate, are given in Table I. According to the literature on this topic,[31,32,50,71] the uncertainties affecting the CCSD(T)/CBS(T,Q)+CV(CT) structures are predicted to be of the order of 0.001–0.002 Å for bond distances and about 0.05°–0.1° for angles.

Figures 1(a) and 1(b) display the most stable conformer of ETSH, i.e., the *gauche* form, and the DMS equilibrium structure, respectively. For *g*-ETSH, the H9S3C1C2 dihedral angle, which defines the conformer, was evaluated to be 61.1°, thus very close to the corresponding parameter of ethanol (62°).[9] The S–C bond distances were found to be 1.8125 Å in *g*-ETSH, 1.8164 Å in *t*-ETSH, and 1.7970 Å in DMS. From the comparison of the *gauche* (*g*) and *trans* (*t*) ETSH structures, it is evident that the g → t conversion process leads to a very small geometry distortion. Only one internal coordinate, the S3C1C2 angle, suffers for a significant variation owing to the SH torsion (∼5°). Dipole moments of the same order of magnitude (see Table I), μ = 1.8086D (*g*-ETSH), μ = 1.7726D (*t*-ETSH), and μ = 1.7633D (DMS), were obtained at the MP2/AVTZ level of theory. These dipole moments are large enough to allow the detection of these species in the ISM by means of radioastronomical observations by exploiting either millimeter-/submillimeter-wave or IR based techniques.

The CCSD(T)/CBS(T,Q)+CV(CT) total electronic energies, −477.914107 a.u. (*g*-ETSH), −477.913368 a.u. (*t*-ETSH), and −477.911632 a.u. (DMS), are also collected in Table I. From their inspection it is evident that DMS is only 543 cm^{-1} less stable than ETSH and the energy difference

TABLE I. Total electronic energies E, relative energies, E_r, and structural parameters[a] of *ethyl mercaptan* and *dimethyl sulfide* calculated at the CCSD(T)/CBS(T,Q)+CV(CT) level.

Ethyl mercaptan				
	gauche	*trans*	Dimethyl sulfide	
E (a.u.)	− 477.914107	− 477.913368	E (a.u.)	− 477.911632
E_r (cm^{-1})	0.0	162.2	θ_1	0.0
θ	− 2.0	0.0	θ_2	0.0
α	− 118.9	0.0	C2S1=C3S1	1.7970
C2C1	1.5173	1.5189	H4C2=H7C3	1.0873
S3C1	1.8125	1.8164	H5C2=H6C2=H8C3=H9C3	1.0885
H4C1	1.0888	1.0877	C3S1C2	98.6
H5C1	1.0894	1.0877	H4C2S1=H7C3S1	107.4
H6C2	1.0905	1.0889	H5C2S1=H6C2S1=H8C3S1=H9C3S1	110.8
H7C2	1.0901	1.0891		
H8C2	1.0889	1.0891	H4C2S1C3=H7C3S1C2	180.0
H9S3	1.3371	1.3363	H5C2S1H4=H8C3S1H7	118.9
S3C1C2	113.6	108.5	H6C2S1H4=H9C3S1H7	− 118.9
H4C1C2	111.1	110.6	μ (D)[b]	1.7633[c]
H5C1C2	110.9	110.6		
H6C2C1	110.5	110.2		
H7C2C1	110.7	110.9		
H8C2C1	110.7	110.9		
H9S3C1	96.6	97.3		
H4C1C2S3	123.4	119.7		
H5C1C2S3	− 117.2	− 119.7		
H6C2C1S3	178.0	180.0		
H7C2C1H6	119.7	119.9		
H8C2C1H6	− 120.5	− 119.9		
H9S3C1C2	61.1	180.0		
μ (D)[b]	1.8086[c]	1.7726[c]		

[a]Distances in Å; angles in degrees.
[b]Dipole moment calculated at the MP2/AVTZ level.
[c]Experimental values: *g*-ETSH = 1.58 ± 0.04 D;[21] *t*-ETSH = 1.61 ± 0.05 D;[21] and DMS = 1.50 ± 0.01 D.[24]

between both ETSH conformers is very small ($\Delta H = 162.2$ cm^{-1}). However, this difference is ten times larger than that observed in ethanol ($\Delta H = 18$ cm^{-1}), for which the *trans* conformer is the favorite structure.[9]

Equilibrium and ground-state rotational constants calculated with different *ab initio* methods are shown in Table II. For comparison purposes, we also quote the experimental data by Schmidt and Quade[21] and Niide and Hayashi.[12]

By using the CCSD(T)/CBS(T,Q)+CV(CT) equilibrium rotational constants, augmented by vibrational corrections from the CCSD/VTZ cubic force field, a very good agreement between theoretical and experimental data is observed, with relative discrepancies of the order of 0.1%. The absolute differences (in MHz) are reported below:

Calc.-expt.	*gauche*-ETSH		*trans*-ETSH		DMS	
ΔA_0	47.13	0.16%	44.07	0.15%	22.72	0.13%
ΔB_0	3.35	0.06%	5.60	0.10%	10.06	0.13%
ΔC_0	2.22	0.05%	4.81	0.10%	7.76	0.14%

From Table II, it is also evident that the explicitly correlated CCSD(T)-F12 method leads to a significant improvement with respect to the CCSD/AVTZ and CCSD(T)/AVTZ equilibrium rotational constants, as was already pointed out by Peterson *et al.*[55] The last comment concerns the core correlation contribution, CV(CT), which turns out to be an important correction and enlarges the rotational constants by about 0.3%–0.5%.

VPT2 anharmonic analysis

Table III shows the harmonic and anharmonic fundamental frequencies calculated with VPT2 and force fields obtained at different levels of theory.

Fundamental vibrations are classified using point group symmetry representations. They are correlated to local modes (although this labeling is ambiguous in relatively complex molecules). Indexes s and t are used for stretching and torsional modes, respectively; the index b (which stands for bending) is used for the remaining modes. Since VPT2 theory is not adequate for treating torsional transitions, anharmonic frequencies are not realistic for these modes. However, VPT2 maps all molecular vibrations and represents a first-order description of what is going on with torsional modes, allowing us to predict Fermi interactions.

TABLE II. Rotational constants of *ethyl-mercaptan* conformers and *dimethyl sulfide* (computed observable parameters noted in boldface).

	gauche-ethyl mercaptan		
	A_e	B_e	C_e
CCSD/AVTZ	28847.09	5293.74	4849.49
CCSD(T)/AVTZ	28651.66	5281.71	4835.54
CCSD(T)-F12/VTZ-F12	28884.87	5327.34	4877.03
CCSD(T)/CBS(T,Q)+CV(CT)	29025.80	5353.12	4900.68
	A_0	B_0	C_0
CCSD(T)/CBS(T,Q)+CV(CT)+ΔB_{vib} (CCSD/VTZ)	**28793.63**	**5298.20**	**4849.04**
Reference 21	28746.37	5294.85	4846.96
	trans-ethyl mercaptan		
	A_e	B_e	C_e
CCSD/AVTZ	28618.93	5477.83	4877.71
CCSD(T)/AVTZ	28407.33	5467.67	4864.97
CCSD(T)-F12/VTZ-F12	28598.92	5519.90	4910.62
CCSD(T)/CBS(T,Q)+CV(CT)	28724.47	5548.90	4936.22
	A_0	B_0	C_0
CCSD(T)/CBS(T,Q)+CV(CT)+ΔB_{vib} (CCSD/VTZ)	**28460.66**	**5491.35**	**4886.62**
Reference 21	28416.59	5485.75	4881.81
	Dimethyl sulfide		
	A_e	B_e	C_e
CCSD/AVTZ	17588.73	7635.73	5710.18
CCSD(T)/AVTZ	17414.21	7635.36	5693.25
CCSD(T)-F12/VTZ-F12	17696.18	7698.18	5756.29
CCSD(T)/CBS(T,Q)+CV(CT)	17828.07	7726.15	5784.64
	A_0	B_0	C_0
CCSD(T)/CBS(T,Q)+CV(CT)+ΔB_{vib} (CCSD/VTZ)	**17832.46**	**7631.16**	**5725.53**
Reference 12	17809.735 (8)	7621.098(2)	5717.769(2)

CCSD/VTZ and CCSD/AVTZ harmonic frequencies and MP2/AVTZ and CCSD/VTZ anharmonic fundamentals are compared in Table III. Several propensity rules can be derived. Generally, the differences between CCSD/AVTZ and CCSD/VTZ frequencies are smaller than 5 cm^{-1}. The CCSD level of theory improves the accuracy with respect to MP2 calculations by displacing the C–H stretching wavenumbers to lower frequencies. Although a general behavior for bending modes cannot be deduced, the highly correlated CCSD method provides the most accurate results. On the basis of *ab initio* calculations, the previous unassigned bands of DMS observed by Durig and Griffin[27] at 1455 cm^{-1} and 1421 cm^{-1} can now be assigned to the $\nu_3(a_1)$ and $\nu_{19}(b_2)$ vibrational modes.

In Table III, the bands strongly displaced by Fermi interactions are emphasized in boldface. For the torsional modes, strong Fermi resonances are not expected in any case. This conclusion is very important for us, since it supports the validity of the two-dimensional model employed in the second part of this paper.

In Table IV, the rotational constants of the ground and torsional excited states, the κ asymmetry parameter, as well as the quartic and sextic centrifugal-distortion constants of the vibrational ground state, employing Watson's *A*-reduced Hamiltonian in the I^r representation, are given. As mentioned in the section titled Theoretical and computational details, equilibrium rotational constants were obtained at the CCSD(T)/CBS(T,Q)+CV(CT) level, while the vibration-rotation interaction constants and sextic centrifugal-distortion constants were determined using cubic CCSD/VTZ force fields. The evaluation of a harmonic force field at the CCSD(T)/VTZ level allowed us to derive accurate quartic centrifugal-distortion constants.

The 2D-potential energy surfaces

The full dimensional anharmonic analysis verified the near independence of the torsional motions with respect to the remaining vibrational modes. This ratifies the validity of the 2D-Hamiltonian of Eq. (3) for the determination of torsional energy levels at low temperatures, provided that small vibrational corrections are considered.

CCSD(T)/AVTZ energies for a grid of 26 non-equivalent geometries were used for the ETSH PES determination. For each grid point, 19 internal coordinates were optimized at the CCSD/AVTZ level. The grid was generated for different values of the dihedral angles H6C2C1S3 (0°, 90°, 180,° and −90° for non-planar structures) and H9S3C1C2 (0°, 30°, 60°, 90°, 120°, 150°, 180°), following the recommendations of Szalay *et al.*[72] Subsequently, the energies were fitted to a symmetry adapted double Fourier series transforming as the totally symmetric representation of the G_6 MSG, after defining the independent coordinates θ and α as

$$\theta = (\text{H6C2C1S3} + \text{H7C2C1S3} + \text{H8C2C1S3})/3 - \pi$$
$$\text{and} \quad \alpha = \text{H9S3C1C2} - \pi.$$

Since formally identical Fourier expansions can be used for $V'(\theta,\alpha)$ and $V^{ZPVE}(\theta,\alpha)$, the final effective PES

TABLE III. Harmonic and anharmonic fundamental frequencies (ω, ν, in cm^{-1}) and intensities (I, in km/mol) of *ethyl-mercaptan* and *dimethyl-sulfide* conformers.[a]

	gauche-ethyl mercaptan							*trans*-ethyl mercaptan							
	MP2 AVTZ ν	CCSD AVTZ ω	CCSD VTZ ω	CCSD VTZ ν	I	Assignment[a]	Expt.[a]		MP2 AVTZ ν	CCSD AVTZ ω	CCSD VTZ ω	CCSD VTZ ν	I	Assignment[a]	Expt.[a]
ν_1	3035	3147	3151	3008	30.2	CH_2-s	2980[b]	a′	3026	3138	3136	2997	29.9	CH_3-s	
ν_2	3017	3125	3127	2989	34.1	CH-s	2967[c]		**3023**	3089	3092	**2990**	9.9	CH_2-s	
ν_3	3008	3121	3126	2986	0.6	CH-s	2930[b]		**2883**	3056	3061	**3016**	23.1	CH_3-s	
ν_4	**3009**	3087	3093	2986	8.2	CH-s	2902[c]		2659	2726	2728	2623	5.6	SH-s	2599[d]
ν_5	**3018**	3050	3054	3009	6.8	CH_3-s	2875[c]		1501	1523	1523	1486	1.9	CH_3-b	
ν_6	2654	2720	2720	2614	5.4	SH-s	2571[c] 2591[d]		1484	1518	1514	1477	5.9	CH_2-b	
ν_7	1494	1521	1517	**1482**	2.4	CH_3-b	1462[c]		1382	1437	1432	**1402**	2.5	CH_3-b	
ν_8	1485	1516	1510	**1479**	15.7	CH_3-b	1452[c]		1268	1323	1322	1318	406.3	CH_2-b	
ν_9	**1463**	1505	1501	**1411**	102.3	CH_2-b	1437[c]		1096	1131	1129	1104	1.1	SCH-b	
ν_{10}	1381	1436	1431	1402	1.1	CH_3-b	1377[c]		**995**	1013	1013	996	2.3	CC-s	
ν_{11}	1278	1329	1327	**1336**	43.9	CH_2-b	1269[c]		854	875	875	865	1.2	HSC-b	
ν_{12}	1261	1301	1298	1277	5.9	CH_2-b	1246[c]		687	695	696	682	1.1	CS-s	
ν_{13}	1102	1139	1135	1109	5.3	HSC-b	1093[c]		303	307	306	305	1.7	SCC-b	
ν_{14}	**1052**	1089	1090	1165	0.0	CH_3-b	1051[c]	a″	3034	3147	3150	3007	32.1	CH-s	
ν_{15}	**978**	1008	1004	974	0.0	CC-s	970[b]		3012	3123	3127	2986	0.5	CH-s	
ν_{16}	868	883	878	870	3.3	HSC-b	867[b]		**1489**	1518	1513	1476	2.3	CH_3-b	
ν_{17}	742	747	747	750	1.2	HSC-b	735[e]		1249	1288	1287	1261	0.4	CH-b	
ν_{18}	672	679	682	**670**	2.9	CS-s	658[b]		**1047**	1063	1060	1090	0.0	CH-b	
ν_{19}	329	331	333	329	1.0	SCC-b	319[c]		787	799	798	796	2.3	CH-b	782[e]
ν_{20}	256	259	264	259	2.6	CH_3-t			249	253	255	248	0.6	CH_3-t	
ν_{21}	194	193	216	218	13.5	SH-t			164	177	179	171	14.6	SH-t	

		Dimethyl sulfide						
		MP2 AVTZ ν	CCSD AVTZ ω	CCSD VTZ ω	CCSD VTZ ν	CCSD VTZ I	Expt.[f]	Assignment[f]
ν_1	a_1	3041	3156	3160	3017	5.8	2997[g]r	CH_3-s
ν_2		**2976**	3055	3059	**2960**	17.5	2925[g]r	CH_3-s
ν_3		1470	1513	1509	**1466**	0.4	1455[g]r	HCH-b
ν_4		1339	1389	1386	**1354**	0.4	1337[g]r	HCH-b
ν_5		1037	1069	1064	1042	8.5	1033[g]r	HCH-b
ν_6		709	717	718	**703**	2.3	696[g]r	CS-s
ν_7		268	267	266	270	0.0	271[g]r	CSC-b
ν_8	a_2	3025	3140	3144	3000	0.0		CH_3-s
ν_9		1438	1490	1485	1446	0.0		CH_3-b
ν_{10}		952	972	966	955	0.0		CH_3-b
ν_{11}		181	182	175	177	0.0		CH_3-t
ν_{12}	b_1	3015	3133	3137	2993	34.7		CH_3-s
ν_{13}		1448	1500	1494	1453	12.4		CH_3-b
ν_{14}		983	1007	1002	986	3.4		CH_3-b
ν_{15}		188	189	187	182	1.0		CH_3-t
ν_{16}	b_2	3043	3157	3161	3017	13.2		CH_3-s
ν_{17}		**2971**	3059	3062	2961	18.0		CH_3-s
ν_{18}		1451	1505	1501	1458	12.3		CH_3-b
ν_{19}		1316	1366	1362	1327	6.4	1421[g]r	CH_3-b
ν_{20}		911	930	924	908	0.3		CH_3-b
ν_{21}		759	771	773	**753**	0.0	740[h]r	CS-s

[a]s = stretching; b = bending; t = torsion; boldface = important Fermi displacements.
[b]Frequencies measured in liquid or solid phase.[14]
[c]IR gas phase.[14]
[d]IR.[15]
[e]IR.[17]
[f]s = stretching; b = bending; t = torsion; boldface = important Fermi displacements; underline = new assignments; r = Raman frequencies, ir = infrared frequencies.
[g]Reference 27.
[h]Reference 11.

TABLE IV. Computed spectroscopic parameters (in MHz) of *ethyl mercaptan* conformers and *dimethyl sulfide*. Equilibrium geometry parameters calculated at the CCSD(T)/CBS(T,Q)+CV(CT) level.[a]

	gauche-ethyl mercaptan	*trans*-ethyl mercaptan	Dimethyl sulfide
κ	−0.962502	−0.948490	−0.677583
A_e	29024.798	28724.466	17828.068
B_e	5353.181	5548.895	7726.148
C_e	4900.879	4936.223	5784.643
	Ground state		Ground state
A_0	28793.630	28460.658	17832.457
B_0	5298.198	5491.347	7631.159
C_0	4849.043	4886.619	5725.527
	Methyl torsion ($\nu = 20$)		Methyl torsion ($\nu = 11$)
ν (cm^{-1})	259	248	177
A_ν	28686.079	28256.193	17822.076
B_ν	5281.251	5474.349	7626.7705
C_ν	4839.216	4877.594	703.770
	SH torsion ($\nu = 21$)		Methyl torsion ($\nu = 15$)
ν (cm^{-1})	218	171	182
A_ν	28774.814	28431.559	17822.389
B_ν	5297.640	5462.784	7655.723
C_ν	4841.012	4881.002	5681.219
	Centrifugal-distortion constants[b]		
Δ_J	0.00336429	0.00376745	0.00860879
Δ_K	0.206297	0.198873	0.139591
Δ_{JK}	−0.0198089	−0.0231073	−0.0390713
δ_J	0.533571×10^{-3}	0.634184×10^{-3}	0.00308610
δ_K	0.00996001	0.0059666	0.00344027
Φ_J	-0.233191×10^{-8}	-0.120387×10^{-7}	-0.485068×10^{-7}
Φ_{JK}	-0.11705×10^{-6}	$.0.466872 \times 10^{-7}$	-0.570882×10^{-7}
Φ_{KJ}	0.86128×10^{-6}	$0.10659061 \times 10^{-5}$	$0.15930388 \times 10^{-5}$
Φ_K	-0.287×10^{-5}	$-0.53975135 \times 10^{-5}$	$-0.44209782 \times 10^{-5}$
ϕ_J	-0.954558×10^{-9}	-0.59071×10^{-8}	-0.240873×10^{-7}
ϕ_{JK}	-0.569409×10^{-7}	$-0.2136158 \times 10^{-6}$	-0.265079×10^{-6}
ϕ_K	0.18000×10^{-5}	$-0.1248905 \times 10^{-5}$	0.7647869×10^{-6}

[a]Vibration-rotation interaction constants at the CCSD/VTZ level.
[b]Parameters obtained using Watson A-reduced Hamiltonian in the I^r representation; quartic centrifugal-distortion constants at the CCSD(T)/VTZ level; and sextic centrifugal-distortion constants at the CCSD/VTZ level.

$(V^{eff}(\theta,\alpha) = V(\theta,\alpha) + V'(\theta,\alpha) + V^{ZPVE}(\theta,\alpha))$ is

$$V^{eff}(\theta,\alpha) = 901.556 - 623.078\cos 3\theta - 10.946\cos 6\theta + 3.577\cos\alpha + 89.650\cos 2\alpha - 256.982\cos 3\alpha - 3.622\cos 4\alpha - 3.322\cos 5\alpha + 1.916\cos 6\alpha + 46.095\cos 3\theta\cos\alpha - 25.618\cos 3\theta\cos 2\alpha + 28.162\cos 3\theta\cos 3\alpha - 1.277\cos 3\theta\cos 4\alpha + 4.439\cos 3\theta\cos 5\alpha - 0.417\cos 3\theta\cos 6\alpha + 4.319\cos 6\theta\cos\alpha - 0.282\cos 6\theta\cos 2\alpha + 1.149\cos 6\theta\cos 3\alpha - 0.324\cos 6\theta\cos 4\alpha - 0.574\cos 6\theta\cos 5\alpha - 0.337\cos 6\theta\cos 6\alpha - 101.387\sin 3\theta\sin\alpha + 2.912\sin 3\theta\sin 2\alpha - 22.510\sin 3\theta\sin 3\alpha + 4.885\sin 3\theta\sin 4\alpha - 7.084\sin 3\theta\sin 5\alpha,$$

where the expansion coefficients for all the cosine and sine terms (type A^{cc} and A^{ss}) are in cm^{-1}. The kinetic energy parameters share symmetry properties with the PES. The A_{00} independent term coefficients were determined to be $A_{00}(B_{\theta\theta}) = 6.1245\ cm^{-1}$, $A_{00}(B_{\alpha\alpha}) = 10.7780\ cm^{-1}$, and $A_{00}(B_{\theta\alpha}) = -0.7427\ cm^{-1}$.

For DMS, we followed a similar procedure. In this case, given the high symmetry, only seven conformations are required: $(\theta_1\theta_2) = (0°,0°)$, $(0°,180°)$, $(180°,180°)$, $(90°,0°)$, $(90°,90°)$, $(90°,180°)$, and $(90°,-90°)$. The two independent coordinates are defined by the following expressions:

$$\theta_1 = (H4C2S1C3 + H5C2S1C3 + H6C2S1C3)/3 - \pi,$$
$$\theta_2 = (H7C3S1C2 + H8C3S1C2 + H9C3S1C2)/3 - \pi.$$

The PES transforms as the totally symmetric representation of the G_{36} group and the effective PES is given by

TABLE V. Potential parameters and internal rotation barriers (in cm^{-1}) calculated at the CCSD(T)/AVTZ level.

	Ethyl mercaptan				Ethanol[9]
	E	$E + E^{ZPVE}$	Expt.[18]	Adjusted	E
V_3 (g)	1174.3	1214.8	1319		1296.3
V_3 (t)	1094.2	1143.4	1319		1226.7
V^{SH} (t → g)	337.2	347.6	359.7		404.1
V^{SH} (g → t)	494.8	523.7	493.4		385.3
V^{SH} (g → g)	466.6	522.4	617.1		423.3
ΔH ($E_t - E_g$)	157.6	176.1	117.7		−18.8
α (g)	118.4°	117.8°	115.2°		118°
		Dimethyl sulfide			Dimethyl ether
V_3	672.0	706.7	745.9[28]	706.7	921[10]
			613.6[12]		757[12]
V(60,60)/2 − V(60,0)	2.3	1.2	51.4	10.8	62[10]

$$V^{\text{eff}}(\theta_1, \theta_2) = 712.532 - 354.641\ (\cos 3\theta_1 + \cos 3\theta_2)$$
$$+0.583 \cos 3\theta_1 \cos 3\theta_2 - 2.767\ (\cos 6\theta_1 + \cos 6\theta_2)$$
$$+0.719\ (\cos 3\theta_1 \cos 6\theta_2 + \cos 6\theta_1 \cos 3\theta_2)$$
$$+0.263 \cos 6\theta 1 \cos 6\theta 2 + 6.075 \sin 3\theta_1 \sin 3\theta_2.$$

The independent coefficients A_{00} of the kinetic energy parameters are $A_{00}(B_{\theta 1\theta 1}) = A_{00}(B_{\theta 2\theta 2}) = 5.8259\ cm^{-1}$ and $A_{00}(B_{\theta 1\theta 2}) = -0.2971\ cm^{-1}$.

In Table V, the CCSD(T)/AVTZ potential parameters of ETSH (see Figure 2) and DMS are compared with previous data calculated for the O-analogs[9,10] and with semi-empirical values derived from microwave, Raman and infrared spectroscopies.[12,18,28] The sets of parameters denoted by E and $E+E^{ZPVE}$ are determined from $V(\theta_1,\theta_2)$ and $V^{eff}(\theta_1,\theta_2)$, respectively. For ETSH, potential energy barriers and the *gauche* SH torsional coordinate $\alpha(g)$ are of the same order of magnitude as in ETOH,[9] whereas for the dimethyl analog V_3 varies from 921 cm^{-1} (DME[10]) to 706.7 cm^{-1} (DMS) upon O → S substitution.

The energy difference 1/2V(60°,60°) − V(60°,0°) quantifies the interactions between the two-methyl groups of DMS. Given the C–O/C–S bond distance ratio, both methyl groups are further away in DMS than in DME. Therefore, they mutually interact slightly in DMS, while they interact strongly in DME. To minimize interactions, the COC bending angle of DME varies with the internal rotation. This fact, reflected in the cubic force field and visible in a test of the occurrence of Fermi resonances, forces the use of a three-dimensional model for the torsional treatment of DME.[10] However, since as is described in the section titled VPT2 anharmonic analysis, perturbations of the DMS torsional levels, due to Fermi interaction with the CSC bending mode, are not expected. The small interactions pointed out for DMS are also reflected in the PES; in fact, the expansion coefficients of the (cos $3\theta_1$ cos $3\theta_2$) and (sin $3\theta_1$ sin $3\theta_2$) terms (0.583 cm^{-1} and 6.075 cm^{-1}) are very small and they are consistent with previous determinations (25.7 cm^{-1} and 6.2 cm^{-1}).[28] The kinetic interaction term $A_{00}(B_{\theta 1\theta 2}) = -0.2971\ cm^{-1}$ compares well with the value by Niide and Hayashi ($B_{\theta 1\theta 2} = -9.6322$ GHz $= -0.3213\ cm^{-1}$).[12]

Far infrared and Raman spectra

Tables VI–VIII report the torsional energy levels calculated variationally as well as the far infrared and Raman transitions. Energy levels are referred to the torsional ZPVE (226.898 cm^{-1} for ETSH and 187.066 cm^{-1} for DMS), and they are classified using the vibrational quanta and the irreducible representations of the G_6 and G_{36} groups of ETSH

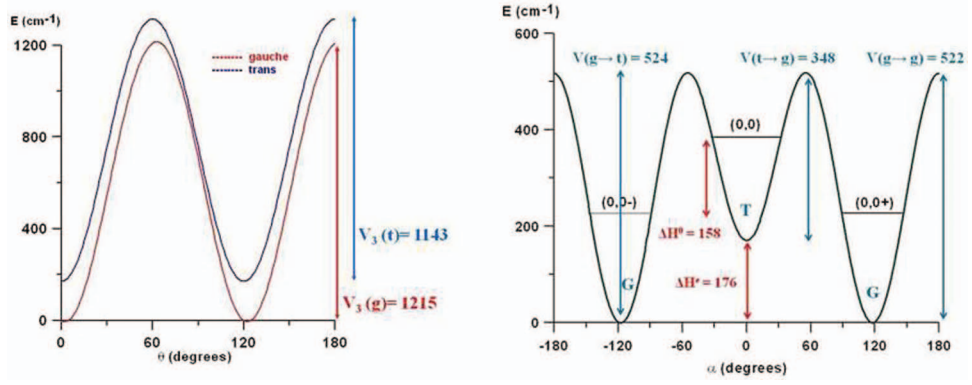

FIG. 2. Torsional energy barriers of ETSH calculated at the CCSD(T)/aug-cc-pVTZ level: (left) methyl torsion barriers; (right) thiol torsion barriers.

TABLE VI. Low torsional energy levels (in cm^{-1}) of ethyl mercaptan and dimethyl sulfide calculated at the CCSD(T)/AVTZ level.

gauche-ethyl mercaptan						*trans*-ethyl mercaptan			Dimethyl sulfide								
ν_{20}, ν_{21}	Symmetry	Calc.	ν_{20}, ν_{21}	Symmetry	Calc.	ν_{20}, ν_{21}	Symmetry	Calc.	ν_{11}, ν_{15}	Symmetry	Calc.	ν_{11}, ν_{15}	Symmetry	Calc.	ν_{11}, ν_{15}	Symmetry	Calc.
0 0^+	A_1	0.000	0 3^+	A_1	480.392	0 0	A_1	157.835	0 0	A_1	0.000	0 2	A_1	361.048	4 0	A_1	578.883
	E	0.000		E	480.393		E	157.835		G	0.001		G	361.044		G	606.512
0 0^-	A_2	0.061	0 3^-	A_2	484.939	0 1	A_2	313.572		E_1	0.001		E_1	361.040		E_1	606.534
	E	0.061		E	484.940		E	313.572		E_3	0.001		E_3	361.039		E_3	606.534
0 1^+	A_1	188.132	2 0^+	A_1	491.359	1 0	A_2	403.069	1 0	A_3	176.516	3 0	A_3	487.696	3 1	A_4	578.840
	E	188.132		E	491.145		E	403.067		G	176.500		G	487.731		G	578.862
0 1^-	A_2	189.613	2 0^-	A_2	491.120	0 2	A_1	424.286		E_2	176.484		E_2	480.630		E_2	606.492
	E	189.613		E	491.384		E	424.286		E_3	176.484		E_3	480.631		E_4	606.492
1 0^+	A_1	254.046	0 4^+	A_1	593.149	1 1	A_1	555.804	0 1	A_2	182.289	2 1	A_2	487.766	2 2	A_1	664.954
	E	254.045		E	593.150		E	555.807		G	182.273		G	480.645		G	659.914
1 0^-	A_2	254.068	0 4^-	A_2	582.960	2 0	A_1	632.303		E_1	182.258		E_1	480.659		E_1	658.846
	E	254.067		E	582.960		E	632.342		E_4	182.258		E_4	480.659		E_3	658.844
0 2^+	A_1	339.848	1 2^+	A_1	609.381	2 1	A_2	780.989	2 0	A_1	339.979	1 2	A_3	516.799	1 3	A_4	669.010
	E	339.848		E	609.383		E	780.861		G	340.213		G	517.050		G	667.404
0 2^-	A_2	356.237	1 2^-	A_2	601.554					E_1	340.587		E_2	517.316		E_2	661.811
	E	356.237		E	601.554					E_3	340.587		E_3	517.316		E_4	661.807
1 1^+	A_1	441.675	2 1^+	A_1	672.804				1 1	A_4	341.312	0 3	A_2	528.202	0 4	A_1	689.205
	E	441.677		E	672.644					G	341.712		G	528.466		G	689.317
1 1^-	A_2	441.334	2 1^-	A_2	670.693					E_2	341.972		E_1	528.713		E_1	689.449
	E	441.336		E	670.604					E_4	341.972		E_4	528.714		E_3	689.441
		ZPVE = 226.898									ZPVE = 187.066						

and DMS, respectively.[9,10] For ETSH, assignments are very arduous because of the large density of interacting states lying at very low energies. Equations (5) and (6) are needed for labeling. The first *trans* level (0 0) lies at 157.835 cm^{-1} above ZPVE (0 0+).

TABLE VII. Torsional transitions (in cm^{-1}) of ETSH.[a]

$(\nu_{20},\nu_{21}) \rightarrow (\nu_{20},\nu_{21})$	Symmetry	Calc.	Expt.
	SH torsion		
	gauche (*g*)		
0 $0^+ \rightarrow$ 0 1^-	$A_1 \rightarrow A_2$	189.6	193.0[b]
0 $0^- \rightarrow$ 0 1^+	$A_2 \rightarrow A_1$	188.0	191.8[b]
0 $1^+ \rightarrow$ 0 2^+	$A_1 \rightarrow A_1$	151.7	157.0[c]
0 $1^- \rightarrow$ 0 2^-	$A_2 \rightarrow A_2$	166.6	169.0[c]
	trans (*t*)		
0 0 $\rightarrow$ 0 1	$A_1 \rightarrow A_2$	157.8	158.0[b]
	CH_3 torsion		
	FIR		
0 $0^+ \rightarrow$ 1 0^-	$A_1 \rightarrow A_2$	254.1 (*g*)	
0 $0^- \rightarrow$ 1 0^+	$A_2 \rightarrow A_1$	254.0 (*g*)	<u>247.5</u>[b]
0 0 $\rightarrow$ 1 0	$A_1 \rightarrow A_2$	<u>245.2 (*t*)</u>	
1 $0^+ \rightarrow$ 2 0^-	$A_1 \rightarrow A_2$	237.1 (*g*)	
1 $0^- \rightarrow$ 2 0^+	$A_2 \rightarrow A_1$	237.4 (*g*)	<u>233.5</u>[b]
1 0 $\rightarrow$ 2 0	$A_2 \rightarrow A_1$	<u>229.2 (*t*)</u>	
	Raman		
0 $0^+ \rightarrow$ 2 0^+	$A_1 \rightarrow A_1$	491.4 (*g*)	
0 $0^- \rightarrow$ 2 0^-	$A_2 \rightarrow A_2$	491.1 (*g*)	482[c]
0 0 $\rightarrow$ 2 0	$A_1 \rightarrow A_1$	474.5 (*t*)	

[a]Underline = new assignments.
[b]Far infrared spectroscopy (FIR).[16]
[c]Raman spectroscopy.[18]

Ethyl mercaptan

Figures 3(a) and 3(b) display the ETSH energies assigned to the SH and CH_3 torsional modes. Each level splits into three sub-components, one non-degenerate A_i (i = 1,2) and two degenerate E, as a consequence of the tunneling effect in the V_3 (g or t) methyl torsional barriers. Furthermore,

TABLE VIII. Non-degenerate components of DMS infrared and Raman transitions (in cm^{-1}).[a]

$(\nu_{11},\nu_{15}) \rightarrow (\nu_{11},\nu_{15})$	Symmetry	CCSD(T)	Adjusted	Expt.[b]
	Infrared transitions			
0 0 $\rightarrow$ 0 1	$A_1 \rightarrow A_2$	182.3	184.9	183.3
0 1 $\rightarrow$ 0 2	$A_2 \rightarrow A_1$	178.8	181.3	180.9
0 2 $\rightarrow$ 0 3	$A_1 \rightarrow A_2$	167.2	169.9	173.1
0 3 $\rightarrow$ 0 4	$A_2 \rightarrow A_1$	161.0	163.6	
1 0 $\rightarrow$ 1 1	$A_3 \rightarrow A_4$	164.8	167.6	<u>168.3</u>
1 1 $\rightarrow$ 1 2	$A_4 \rightarrow A_3$	175.5	177.9	
1 2 $\rightarrow$ 1 3	$A_3 \rightarrow A_4$	152.2	154.6	
2 0 $\rightarrow$ 2 1	$A_2 \rightarrow A_2$	147.8	150.1	
2 1 $\rightarrow$ 2 2	$A_2 \rightarrow A_1$	177.2	179.6	
	Raman transitions			
0 0 $\rightarrow$ 0 2	$A_1 \rightarrow A_1$	361.1	366.2	365
0 1 $\rightarrow$ 0 3	$A_2 \rightarrow A_2$	345.9	351.2	354
0 2 $\rightarrow$ 0 4	$A_1 \rightarrow A_1$	328.2	333.5	
0 0 $\rightarrow$ 2 0	$A_1 \rightarrow A_1$	340.0	345.1	344
1 0 $\rightarrow$ 3 0	$A_3 \rightarrow A_3$	311.2	316.2	
2 0 $\rightarrow$ 4 0	$A_1 \rightarrow A_1$	238.9	245.6	

[a]Underline = new assignments.
[b]Reference 28.

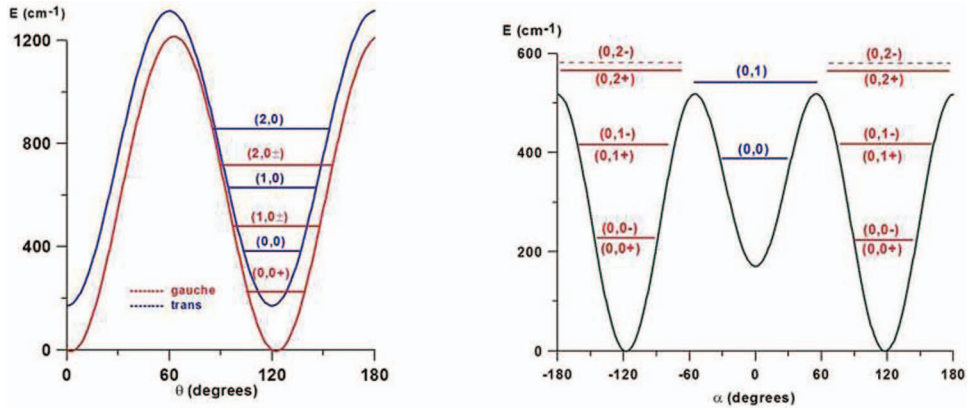

FIG. 3. Torsional energy levels of ETSH: (left) methyl torsional energy levels; (right) thiol torsional energy levels.

in *g*-ETSH, the barrier separating the two equivalent *gauche* minima, V(g → g), splits the A_i and E sub-levels into two components + and −. As was expected given the barriers heights ($V_3(g)$ = 1214.8 cm^{-1}; $V_3(t)$ = 1143.4 cm^{-1}), energy gaps between A_i and E sub-levels are unnoticeable below the methyl overtones. The E(0 0^+)–E(0 0^-) splitting of the g ground state is 0.06 cm^{-1} (V(g → g) = 522.4 cm^{-1}).

As was first pointed out for ethanol,[9] calculations show large differences between the *gauche* and *trans* ethyl mercaptan spectral features. Band superpositions are unachievable. Interactions between rotating groups cause displacements of the *g*-bands with respect to the *t*-bands that cannot be described with one-dimensional models. Non-bonding interactions among SH and CH_3 hydrogen atoms are more relevant in the *g*-ETSH form. The *g*-ETSH fundamental transitions were localized at 188.132 cm^{-1} and 189.613 cm^{-1} (SH torsion) and 254.046 cm^{-1} and 254.068 cm^{-1} (CH_3 torsion). In *t*-ETSH, they lie at 155.737 cm^{-1} (SH torsion) and at 245.234 cm^{-1} (CH_3 torsion) over the (0,0) *trans*-level. From the comparison of these data with the VTP2 results of Table III, it may be inferred that the latter theory provides reasonable frequencies for the methyl torsion but it is unreliable for the SH torsion.

For *g*-ETSH, (0 $2^{\pm}$) splits into two components (0 2^+) and (0 2^-) lying at 339.848 cm^{-1} and 356.237 cm^{-1}, respectively, thus separated by 16.4 cm^{-1}. This splitting was measured to be 12 cm^{-1} by Raman spectroscopy[18] and arises from resonances between (0 2^+) and the (0 2) *t*-level. For the methyl rotation, the A_1 and E (2 0) levels lie at 474.468 cm^{-1} and 474.507 cm^{-1} above (0,0), respectively, while the A_1 and E (2 0^+) ones lie at 491.359 cm^{-1} and 491.145 cm^{-1} above (0 0+). Anharmonic effects can be estimated using the $2\nu_{20}/\nu_{20}$ and $2\nu_{21}/\nu_{21}$ ratios, and they are more relevant for the SH torsion than for the CH_3 torsion.

Table VII collects the ETSH torsional transitions compared with the experimental far infrared frequencies[16] and the Raman spectra of overtones.[18] Observed infrared data correspond to c-type bands whose intensities depend on the out-of-plane component of the dipole moment. For the SH torsion, there is a very good agreement between calculated and experimental data. The differences are smaller than 5 cm^{-1} for the *gauche* conformer levels and even smaller (0.2 cm^{-1}) for the *trans*-fundamental.

With respect to the CH_3 torsion, the comparison is not straightforward since previous experimental analysis did not distinguish among *gauche* and *trans* levels. Furthermore, one-dimensional models were used for spectra reduction and assignments,[18,25] thus neglecting the combination bands. Our *trans* levels at 245.2 cm^{-1} and 229.2 cm^{-1} are closer to the experimental values than our results for the *gauche* conformer. Our calculations support assignments of the overtone observed at 482 cm^{-1} to two very different calculated transitions: either the *gauche*-overtone (491.4 cm^{-1} and 491.1 cm^{-1}) or the *trans*-overtone (474.5 cm^{-1}). Both assignments are affected by errors of ∼8 cm^{-1}. In general calculated overtones using our model are less accurate than fundamentals. This supports the assignment of the band observed at 247.5 cm^{-1} to the CH_3 fundamental of the *trans* conformer.

In the section titled Dimethyl-sulfide: *Ab initio* calculations and fit, a fit of DMS spectra is described. We have avoided this procedure for ETSH because of the uncertainties in the experimental assignments. Furthermore, we used a 2D-model and, to our knowledge, there are no experimental data available concerning combination bands.

Dimethyl-sulfide: Ab initio calculations and fit

In DMS, whose V_3 barrier (706.7 cm^{-1}) is lower than that of ETSH, torsional splittings are already visible in the fundamentals. Since the PES displays nine equivalent minima, each torsional level splits into nine components, one non-degenerate A_i (A_i = 1,2,3,4), four components in the two-fold degenerate E_i (i = 1,2) and E_j (j = 3,4) symmetries and four in the degenerate G symmetry.[10]

Tables VI and VIII collect the torsional levels and transitions. The non-degenerate components of the torsional levels (1,0) and (0,1) were calculated to be 176.516 cm^{-1} (ν_{11}) and 182.289 cm^{-1} (ν_{15}), i.e., very close to the CCSD/VTZ fundamentals predicted to lie at 177 cm^{-1} and 182 cm^{-1} using VPT2 (see Table III). ν_{15} is infrared active and its intensity depends on the out-of-plane component of the dipole moment. The new predicted transitions represent an important

improvement with respect to previous data[30] calculated from a MP2 PES neglecting the vibrational corrections and using a basic definition of the independent coordinates.

For ν_{15}, the differences between theory and experiment for the fundamental 0 0 → 0 1 and the first sequence 0 1 → 0 2 are very small (1 cm^{-1} and 2.1 cm^{-1}). The two overtones $2\nu_{15}$ and $2\nu_{11}$, calculated to be 361.1 cm^{-1} and 340 cm^{-1}, are also very close to the experimental data (365 cm^{-1} and 344 cm^{-1}). In addition, we obtained a very good agreement for the gap $2\nu_{15} - 2\nu_{11}$ (21.1 cm^{-1}) and the corresponding experimental value (21 cm^{-1}) that demonstrates how accurate are the kinetic and potential terms of Eq. (3) responsible for the separation of the two torsional modes. In particular, these are the A^{ss} coefficient of the ($\sin 3\theta_1 \sin 3\theta_2$) term of the PES (6.075 cm^{-1}) and the $B_{\theta 1 \theta 2}$ kinetic energy parameter ($A_{00}(B_{\theta 1 \theta 2}) = -0.2971$ cm^{-1}).

In the far infrared spectrum of DMS[28] there is an unlabeled band observed at 168.3 cm^{-1}. It has been tentatively assigned to the excited 0 3 → 0 4 transition and to the 1 0 → 1 1 combination band. To solve any possible discrepancy in its assignment, we have performed an empirical adjustment of the *ab initio* PES. For this purpose, *ab initio* data have been used as starting point of a linear fit of the other six experimental frequencies of Table VIII. A considerable improvement of the computed frequencies was already obtained with the fit of only one potential parameter.

In the fit, a small variation of the ($\cos 3\theta 1 + \cos 3\theta 2$) term coefficient from −354.641 cm^{-1} to −364.021 cm^{-1} is noted. This reduces the RMS of the fit by about 50% (from 4.461 cm^{-1} to 1.988 cm^{-1}). Such an improvement is sufficient to assign the band recorded at 168.3 cm^{-1} to the 1 0 → 1 1 combination transition. The improved surface is given by the following expression:

$$
\begin{aligned}
V^{\mathrm{ADJ}}(\theta_1,\theta_2) = {} & 712.532 - 364.021\,(\cos 3\theta_1 + \cos 3\theta_2) \\
& + 0.583 \cos 3\theta_1 \cos 3\theta_2 - 2.767\,(\cos 6\theta_1 + \cos 6\theta_2) \\
& + 0.719\,(\cos 3\theta_1 \cos 6\theta_2 + \cos 6\theta_1 \cos 3\theta_2) \\
& + 0.263 \cos 6\theta 1 \cos 6\theta 2 + 6.075 \sin 3\theta_1 \sin 3\theta_2 .
\end{aligned}
$$

In this fit, 1 0 → 1 1 is predicted at 167.6 cm^{-1}, while the non-degenerate component of 0 3 → 0 4 lies at 163.6 cm^{-1}. It is supposed that the latter transition provides a broad band because the degenerated components are computed at 158.4 cm^{-1} (G → G and $E_3 \rightarrow E_4$), and at 158.7 cm^{-1} ($E_1 \rightarrow E_1$). Furthermore, it should be pointed out that the value of the fitted parameter value increases V(60,60) (Table V) by about 19 cm^{-1}. Therefore, the fitted value of the torsional barrier is going in the direction of the experimental value of Durig *et al.*[28]

CONCLUSIONS

By using the CCSD(T)/CBS(T,Q)+CV(CT) level of theory, the structures of the two conformers of ETSH and that of DMS have been determined. DMS is only 543 cm^{-1} less stable than ETSH. The *t*-ETSH *trans* conformer lies 162.2 cm^{-1} above the most stable *gauche* structure. This energy difference is ten times larger than that observed in ethanol, for which the *trans* form was established to be the favorite geometry.

CCSD/VTZ vibration-rotation interaction constants in conjunction with best-estimated equilibrium rotational constants have been used to obtain the following rotational constants for the vibrational ground state: $A_0 = 28793.63$ MHz, $B_0 = 5298.20$ MHz, $C_0 = 4849.04$ MHz for *g*-ETSH, $A_0 = 28460.66$ MHz, $B_0 = 5491.35$ MHz, $C_0 = 4886.62$ MHz for *t*-ETSH, and $A_0 = 17832.46$ MHz, $B_0 = 7631.16$ MHz, $C_0 = 5725.53$ MHz for *g*-DMS.

The full-dimensional anharmonic analysis does not predict displacements of the lowest torsional excited states due to Fermi resonances with the remaining vibrational modes. The DMS Raman bands observed at 1455 cm^{-1} and 1421 cm^{-1} are assigned to the $\nu_3(a_1)$ and $\nu_{19}(b_2)$ vibrational modes.

Torsional transitions and splittings have been calculated variationally using two-dimensional models and CCSD/AVTZ two-dimensional potential energy surfaces. Calculations show large differences between *gauche* and *trans* ethyl mercaptan spectral torsional features. Band superposition is thus unachievable. Interactions between rotating groups cause displacements of the *g*-bands with respect to the *t*-bands that cannot to be described with one-dimensional models. New assignments are proposed for the methyl torsion bands of ETSH. A reassignment of the observed infrared bands of DMS (0 3 → 0 4 and 1 0 → 1 1) is also suggested.

ACKNOWLEDGMENTS

This research was supported by a Marie Curie International Research Staff Exchange Scheme Fellowship within the 7th European Community Framework Program under Grant No. PIRSES-GA-2012-31754, the COST Action CM1002 CODECS, and the FIS2011-28738-C02-02 project (MINECO, Spain). In Bologna, this work was supported by MIUR (PRIN 2009 funds) and by the University of Bologna (RFO funds).

The authors acknowledge the CTI (CSIC) and CESGA for computing facilities.

[1] S. M. Fortman, I. R. Medvedev, C. F. Neese, and F. C. De Lucia, Astrophys. J. Lett. **725**, L11 (2010).
[2] E. Herbst and E.-F. van Dishoeck, Annu. Rev. Astron. Astrophys. **47**, 427 (2009).
[3] J. Cernicharo, C. Kahane, M. Guélin, and H. Hein, Astron. Astrophys. **181**, L9 (1987).
[4] A. Penzias, P. M. Solomon, R. W. Wilson, A. A. Penzias, and K. B. Jefferts, Astrophys. J **168**, L53 (1971).
[5] S. B. Charnley, Astrophys. J. **481**, 396 (1997).
[6] V. Wakelam, P. Caselli, C. Ceccarelli, E. Herbst, and A. Castets, Astron. Astrophys. **422**, 159 (2004).
[7] J. Hatchell, M. A. Thompson, T. J. Millar, and G. H. Macdonald, Astron. Astrophys. **338**, 713 (1998).
[8] R. A. Linkem, M. A. Freeking, and P. Thaddeus, Astrophys. J. **234**, L139 (1979).
[9] M. L. Senent, Y. G. Smeyers, R. Dominguez-Gómez, and M. Villa, J. Chem. Phys. **112**, 5809 (2000).
[10] M. Villa, M. L. Senent, R. Domínguez-Gómez, O. Álvarez-Bajo, and M. Carvajal, J. Phys. Chem. A **115**, 13573 (2011).
[11] R. Fonteyne, J. Chem. Phys. **8**, 60 (1940).
[12] Y. Niide and M. Hayashi, J. Mol. Spectrosc. **223**, 152 (2004).
[13] N. Sheppard, J. Chem. Phys. **17**, 79 (1949).
[14] D. Smith, J. P. Devlin, and D. W. Scott, J. Mol. Spectrosc. **25**, 174 (1968).

[15]B. J. Miller, D. L. Howard, J. R. Lane, H. G. Kjaergaard, M. E. Dunn, and V. Vaida, J. Phys. Chem. A. **113**, 7576 (2009).
[16]A. S. Manocha, W. G. Fateley, and T. Shimanouchi, J. Phys. Chem. **77**, 1977 (1973).
[17]H. Wolff and J. Szydlowski, Can. J. Chem., **63**, 1708 (1985).
[18]J. R. Durig, W. W. Bucy, C. J. Wurrey, and L. A. Carreira, J. Phys. Chem. **79**,988 (1975).
[19]W. Richter and W. D. Schiel, Chem. Phys. Lett. **108**, 480 (1984).
[20]F. Inagaki, I. Harada, and T. Shimanouchi, J. Mol. Spectrosc. **46**,381 (1973).
[21]R. E. Schmidt and C. R. Quade, J. Chem. Phys. **62**, 3864 (1975).
[22]C. Sosa, R. J. Bartlett, K. KuBulat, and W. B. Person, J. Phys. Chem. **93**, 577 (1989).
[23]S. Choi, T. Y. Kang, K.-W. Choi, S. Han, A.-S. Ahn, S. J. Baek, and S. K. Kim, J. Phys. Chem. A. **112**, 7191 (2008).
[24]L. Pierce and M. Hayashi, J. Chem. Phys. **35**, 479 (1961).
[25]J. Demaison, D. Schwoch, B. T. Tan, and H. D. Rudolph, J. Mol. Spectrosc. **83**, 391 (1980).
[26]J. M. Vacherand, G. Wlodarczak, A. Dubrulle, and J. Demaison, Can. J. Phys. **65**, 1159 (1987).
[27]J. R. Durig and M. G. Griffin, J.Chem. Phys. **67**, 2230 (1977).
[28]J. R. Durig, M. R. Jabilan, J. F. Sullivan, and D. A. C. Compton, J. Chem. Phys. **75**, 4833 (1981).
[29]R. Fausto, J. J. C. Teixeira-Dias, and P. R. Carey, J. Mol. Struct. **159**, 137 (1987).
[30]M. L. Senent, D. C. Moule, and Y. G. Smeyers, J. Phys. Chem. **99**, 7970 (1995).
[31]M. Heckert, M. Kállay, and J. Gauss, Mol. Phys. **103**, 2109 (2005).
[32]M. Heckert, M. Kállay, D. P. Tew, W. Klopper, and J. Gauss, J. Chem. Phys. **125**, 044108 (2006).
[33]M. L. Senent, ENEDIM, A variational code for non-rigid molecules, 2001, see http://tct1.iem.csic.es/senent/PROGRAMAS.htm, for more details.
[34]Y. G. Smeyers, M. L. Senent, V. Botella, and D. C. Moule, J. Chem. Phys. **98**, 2754 (1993).
[35]D. C. Moule, Y. G. Smeyers, M. L. Senent, D. J. Clouthier, J. Karolczak, and R. Judge, J. Chem. Phys. **95**(5), 3137–3146 (1991).
[36]M. L. Senent and Y. G. Smeyers, J. Chem. Phys. **105**, 2789 (1996).
[37]CFOUR, a quantum chemical program package written by J. F. Stanton, J. Gauss, M. E. Harding, P. G. Szalay with contributions from A. A. Auer, R. J. Bartlett, U. Benedikt, C. Berger, D. E. Bernholdt, Y. J. Bomble, L. Cheng, O. Christiansen, M. Heckert, O. Heun, C. Huber, T.-C. Jagau, D. Jonsson, J. Jusélius, K. Klein, W. J. Lauderdale, D. A. Matthews, T. Metzroth, L. A. Mück, D. P. O'Neill, D. R. Price, E. Prochnow, C. Puzzarini, K. Ruud, F. Schiffmann, W. Schwalbach, S. Stopkowicz, A. Tajti, J. Vázquez, F. Wang, J. D. Watts; the integral packages MOLECULE (J. Almlöf and P. R. Taylor), PROPS (P. R. Taylor), ABACUS (T. Helgaker, H. J. Aa. Jensen, P. Jørgensen, and J. Olsen), and ECP routines by A. V. Mitin and C. van Wüllen, see http://www.cfour.de.
[38]K. Raghavachari, G. W. Trucks, J. A. Pople, and M. Head-Gordon, Chem. Phys. Lett. **157**, 479 (1989).
[39]T. H. Dunning, Jr., J. Chem. Phys. **90**, 1007 (1989).
[40]D. E. Woon and T. H. Dunning, Jr., J. Chem. Phys. **103**, 4572 (1995).
[41]K. A. Peterson and T. H. Dunning, Jr., J. Chem. Phys. **117**, 10548 (2002).
[42]D. Feller, J. Chem. Phys. **98**, 7059 (1993).
[43]T. Helgaker, W. Klopper, H. Koch, and J. Noga, J. Chem. Phys. **106**, 9639 (1997).
[44]I. M. Mills, in *Molecular Spectroscopy: Modern Research*, edited by K. N. Rao and C. W. Mathews (Academic Press, New York, 1972).
[45]J. Gauss and J. F. Stanton, Chem. Phys. Lett. **276**, 70 (1997).
[46]W. Schneider and W. Thiel, Chem. Phys. Lett. **157**, 367 (1989).
[47]J. F. Stanton, C. L. Lopreore, and J. Gauss, J. Chem. Phys. **108**, 7190 (1998).
[48]M. R. Aliev and J. K. G. Watson, in *Molecular Spectroscopy: Modern Research*, edited by K. N. Rao (Academic Press, New York, 1985), Vol. III, p. 1.
[49]C. Puzzarini, M. Heckert, and J. Gauss, J. Chem. Phys. **128**, 194108 (2008).
[50]C. Puzzarini, J. F. Stanton, and J. Gauss, Int. Rev. Phys. Chem. **29**, 273 (2010).
[51]C. Puzzarini, G. Cazzoli, J. C. López, J. L. Alonso, A. Baldacci, A. Baldan, S. Stopkowicz, L. Cheng, and J. Gauss, J. Chem. Phys. **137**, 024310 (2012).
[52]G. Knizia, T. B. Adler, and H.-J. Werner, J. Chem. Phys. **130**, 054104 (2009).
[53]H.-J. Werner, T. B. Adler, and F. R. Manby, J. Chem. Phys. **126**, 164102 (2007).
[54]H.-J. Werner, P. J. Knowles, F. R. Manby, and M. Schütz, MOLPRO, version 2010.1, a package of *ab initio* programs, 2010, see http://www.molpro.net.
[55]K. A. Peterson, T. B. Adler, and H.-J. Werner, J. Chem. Phys. **128**, 084102 (2008).
[56]F. Weigend, Phys. Chem. Chem. Phys. **4**, 4285 (2002).
[57]C. Hättig, Phys. Chem. Chem. Phys. **7**, 59 (2005).
[58]W. Klopper, Mol. Phys. **99**, 481 (2001).
[59]K. E. Yousaf and K. A. Peterson, J. Chem. Phys. **129**, 184108 (2008).
[60]R. A. Kendall, T. H. Dunning, Jr., and R. J. Harrison, J. Chem. Phys. **96**, 6796 (1992).
[61]M. Hochlaf, R. Linguerri, S. S. Dalal, and J. S. Francisco, J. Chem. Phys. **136**, 244311 (2012).
[62]V. Brites and M. Hochlaf, J. Phys. Chem. A **113**, 11107 (2009).
[63]F. Lique, J. Klos, and M. Hochlaf, Phys. Chem. Chem. Phys. **12**, 15672 (2010).
[64]G. Rauhut, G. Knizia, and H.-J. Werner, J. Chem. Phys. **130**, 054105 (2009).
[65]Y. Ajili, K. Hammami, N. E. Jaidane, M. Lanza, Y. N. Kalugina, F. Lique, and M. Hochlaf, Phys. Chem. Chem. Phys. **15**, 10062 (2013).
[66]O. Yazidi and M. Hochlaf, Phys. Chem. Chem. Phys. **15**, 10158 (2013).
[67]M. L. Senent, Chem. Phys. Lett., **296**, 299 (1998).
[68]M. L. Senent, J. Mol. Spectros. **191**, 265 (1998).
[69]M. J. Frisch, G. W. Trucks, H. B. Schlegel *et al.*, GAUSSIAN 09, Revision A.1, Gaussian, Inc., 2009.
[70]A. G. Császár, V. Szalay, and M. L. Senent, J. Chem. Phys. **120**, 1203 (2004).
[71]V. Barone, M. Biczysko, J. Bloino, and C. Puzzarini, Phys. Chem. Chem. Phys. **15**, 10094 (2013).
[72]V. Szalay, A. G. Császár, and M. L. Senent, J. Chem. Phys. **117**, 6489 (2002).